



Insights into the cyclic voltammetry of surface-confined molecules undergoing two-electron transfers of any reversibility and any ordering of the formal potentials: Unravelling the apparent governing factors

Manuela López-Tenés^{*}, Joaquín González, Eduardo Laborda, Angela Molina

Departamento de Química Física, Facultad de Química, Regional Campus of International Excellence "Campus Mare Nostrum", Universidad de Murcia, Murcia 30100, Spain

ARTICLE INFO

Keywords:

Surface EE mechanism
Electron transfer kinetics
Apparent rate constants
Cyclic voltammetry
Quantitative analysis

ABSTRACT

The cyclic voltammetry (CV) of surface-immobilized electroactive species undergoing two-electron transfers (so-called surface EE mechanism) is comprehensively studied in this work, considering any electron transfer kinetics (k_1^0, k_2^0) and any values of their formal potentials (E_1^0, E_2^0). Hence, a large number of possible situations arise, which are systematized through the definition of apparent electrochemical rate constants for both electron transfers (which account for the combined effect of k_i^0 ($i = 1, 2$), $\Delta E^0 (= E_2^0 - E_1^0)$ and the scan rate), with their values and ratio determining the features of the voltammetric signal.

Guidelines are established for the elucidation of the reversibility of the process as a function of the relative values of such apparent rate constants, which reflects on the symmetry of the CV signals in the forward and reverse scans. Thus, as the second transfer is more favorable than the first one, kinetically and/or thermodynamically, the process behaves as more irreversible. Also, simple protocols of quantification of the corresponding kinetic and thermodynamic parameters are given on the basis of the analysis of the height, width, number and position of the CV peaks.

1. Introduction

Molecules undergoing multi-electron transfers are highly relevant in a number of scientific and technological fields including the (bio) catalysis of electrochemical reactions [1,2], electrosynthesis of new compounds and materials [3–6], activity of organometallic anticancer agents [7], molecular electronics [8], electroanalysis [9],... In many cases, the redox (bio)molecule is immobilized on a conductive substrate in order to improve their stability, facilitate their recovery, and 'tune' the electron transfer (ET) rates, which can increase the sensitivity, reproducibility and selectivity of the electrochemical response [10,11].

The features of redox films are typically tested via voltammetric methods, specifically by cyclic voltammetry (CV) [1,12,13]. Interestingly though, theoretical models and procedures of analysis of voltammetric data of surface-confined redox species are scarce in the literature [14], especially with regard to the more general and frequent situation of non-reversible ETs. Indeed, in a limited number of works by Hubbard [15], Laviron [16], Oldham [17] and Maldonado [18] is the behavior of

quasireversible mono-electron transfers investigated. Regarding non-reversible multi-electron transfers, to the best of our knowledge, theoretical studies are restricted to contributions by Bond [19,20], Gulaboski [21,22], and the analytical theory obtained by our group for the two-electron transfer of surface-bound species (surface EE mechanism) [23].

Attending to the above, this work includes a comprehensive investigation of the CV of the surface EE mechanism. The study does not presuppose neither electrochemical reversibility, nor the normal ($E_1^0 > E_2^0$) or inverted ($E_1^0 < E_2^0$) ordering of the formal potentials [24]. Instead, it presents a complete analysis on how the kinetics of the first and second ETs affect the features of the current-potential (I/E) signal. The chief parameters of the voltammetric behavior in the different kinetic regimes (reversible, quasireversible and irreversible) are identified, defining 'apparent' kinetic rate constants of the ETs that account for the entangled influence of both kinetic and thermodynamic factors, as well as of the experimental scan rate. In most cases, by appropriate experimental design and scrutiny of the shape, magnitude and symmetry

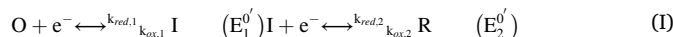
^{*} Corresponding author.

E-mail address: manuela@um.es (M. López-Tenés).

of the cyclic voltammograms, such factors can be unraveled so that the individual values of the standard heterogeneous rate constants and the formal potentials can be determined. For this, guidelines and suitable protocols are provided in this work, pointing out the key influence of the ratio between the apparent rate constants of the two ETs. Systems of special experimental relevance on which the theoretical formalism here presented can be applied are, among others, quinone and anthraquinone moieties [25], flavins [26], polyoxometalates [27] and redox protein and enzymes [28].

2. Theory

Let us consider a surface process where a surface-immobilized species O can be electro-reduced according to the following EE mechanism:



with O (oxidized), I (intermediate, or half-reduced) and R (reduced) referring to the different redox states of adsorbed molecule O, $k_{red,i}$ and $k_{ox,i}$ are the heterogeneous charge transfer rate constants for the reduction and oxidation processes, respectively, of step i ($i = 1, 2$), and $E_1^{0'}$ and $E_2^{0'}$ are the formal potentials of the first and second steps, respectively. The average formal potential, $\bar{E}^{0'}$, is given by:

$$\bar{E}^{0'} = \frac{E_1^{0'} + E_2^{0'}}{2} \quad (1)$$

Also, a key parameter in the study of the EE process is the difference between the formal potentials, $\Delta E^{0'}$, defined as:

$$\Delta E^{0'} = E_2^{0'} - E_1^{0'} \quad (2)$$

In reference [23], an analytical expression for the CV response of the surface EE mechanism given in reaction scheme (I) was obtained for any degree of reversibility and for any ordering of the formal potentials (either normal, $\Delta E^{0'} < 0$, or inverted, $\Delta E^{0'} > 0$ [24]), under the assumptions that the adsorption of molecule O follows the Langmuir isotherm, the heterogeneity of the electroactive monolayer can be ignored and no desorption takes place in the time scale of the experiment. Thus, the current associated to process (I) when a CV perturbation is applied (equivalent to a sequence of constant potentials E^1, E^2, \dots, E^{np} of duration τ with a small pulse amplitude, $\Delta E < 0.001\text{mV}$ [23]) is given by:

$$\frac{I_{CV}^p}{Q_F} = \delta^p K_1^p \vartheta_1^p - \gamma^p K_2^p \vartheta_2^p \quad p = 1, 2, \dots, np \quad (3)$$

with δ^p and γ^p being coefficients given in Section SII of Supporting Information (SI) for any kinetic model,

$$\vartheta_i^p = \exp(-K_i^p \tau) \quad i = 1, 2; \quad p = 1, 2, \dots, np \quad (4)$$

where

$$K_i^p = k_{red,i}^p + k_{ox,i}^p \quad i = 1, 2; \quad p = 1, 2, \dots, np \quad (5)$$

and

$$Q_F = F S \Gamma_T \quad (6)$$

with F being the Faraday constant, S the electrode area and Γ_T the total excess.

Hereafter, the Butler-Volmer kinetic model will be assumed so that the rate constants for reduction and oxidation processes are given by [12,13,29]:

$$\left. \begin{aligned} k_{red,i}^p &= k_i^{0'} e^{-\alpha f (E^p - E_i^{0'})} \\ k_{ox,i}^p &= k_i^{0'} e^{(1-\alpha)f (E^p - E_i^{0'})} \end{aligned} \right\} \begin{aligned} &i = 1, 2 \\ &p = 1, 2, \dots, np \end{aligned} \quad (7)$$

where $k_i^{0'}$ is the standard heterogeneous rate constant for the ET corresponding to step i ($i = 1, 2$), α is the charge transfer coefficient, assumed equal for both ETs, and

$$f = \frac{F}{RT} \quad (8)$$

with R and T having their usual meaning.

In CV, it is appropriate to introduce the following dimensionless variables:

$$\psi_{CV} = \frac{I_{CV}}{Q_F a} \quad (9)$$

$$k_{i,CV}^{0'} = \frac{k_i^{0'}}{a} \quad i = 1, 2 \quad (10)$$

$$a = v f \quad (11)$$

where v is the scan rate, and for the sake of simplicity the superscript p has been, and will be hereafter, omitted.

Attending to the central importance of the average formal potential, $\bar{E}^{0'}$ (Eq. (1)), in the behavior of an EE mechanism [13,23,30], the reduction and oxidation rate constants for both ETs (Eqs. (7)), and taking into account Eq. (10), can be re-written as follows:

$$\begin{aligned} k_{red,1,CV} &= k_{1,CV}^{0'} e^{-\alpha f \frac{\Delta E^{0'}}{2}} e^{-\alpha f (E - \bar{E}^{0'})} \\ k_{ox,1,CV} &= k_{1,CV}^{0'} e^{(1-\alpha)f \frac{\Delta E^{0'}}{2}} e^{(1-\alpha)f (E - \bar{E}^{0'})} \\ k_{red,2,CV} &= k_{2,CV}^{0'} e^{\alpha f \frac{\Delta E^{0'}}{2}} e^{-\alpha f (E - \bar{E}^{0'})} \\ k_{ox,2,CV} &= k_{2,CV}^{0'} e^{-(1-\alpha)f \frac{\Delta E^{0'}}{2}} e^{(1-\alpha)f (E - \bar{E}^{0'})} \end{aligned} \quad (12)$$

which clearly show the intrinsic influence of $\Delta E^{0'}$ (Eq. (2)) in the definitions of the electrochemical rate constants of mechanism (I). Thus, from Eq. (12), two apparent heterogeneous rate constants can be defined both for the reduction and the oxidation processes. For $\alpha = 0.5$, they fulfill that:

$$\begin{aligned} \left(k_{1,CV,app}^{0'} \right)_{red} &= k_{1,CV}^{0'} e^{-\frac{f \Delta E^{0'}}{2}} = \left(k_{2,CV,app}^{0'} \right)_{ox} 10^{-R_k} \\ \left(k_{2,CV,app}^{0'} \right)_{red} &= k_{2,CV}^{0'} e^{\frac{f \Delta E^{0'}}{2}} = \left(k_{1,CV,app}^{0'} \right)_{ox} 10^{R_k} \end{aligned} \quad (13)$$

Eq. (13) show that the overall rate of an EE process is determined by the values of $k_{1,CV}^{0'}$, $k_{2,CV}^{0'}$ and $\Delta E^{0'}$. Also, the CV response depends on the ratio between $k_{1,CV}^{0'}$ and $k_{2,CV}^{0'}$ through the parameter R_k , defined as the common logarithm of their ratio [23],

$$R_k = \log \left(\frac{k_{2,CV}^{0'}}{k_{1,CV}^{0'}} \right) \quad (14)$$

so that from Eqs. (13) and (14) it is derived that:

$$\begin{aligned} R_{k,app,red} &= \log \left(\frac{k_{2,CV,app}^{0'}}{k_{1,CV,app}^{0'}} \right)_{red} = R_k + \frac{0.5f}{2.3} \Delta E^{0'} \\ R_{k,app,ox} &= \log \left(\frac{k_{2,CV,app}^{0'}}{k_{1,CV,app}^{0'}} \right)_{ox} = R_k - \frac{0.5f}{2.3} \Delta E^{0'} \end{aligned} \quad (15)$$

It is worth pointing out that, just by careful inspection of Eq. (12) and without any further theoretical development, the two following

predictions become obvious for the most typical value of $\alpha = 0.5$, independently of the reversibility of the two ETs:

1 Provided that

$$\begin{aligned} k_{red,1,CV}(E) &= k_{ox,2,CV}(-E) \\ k_{red,2,CV}(E) &= k_{ox,1,CV}(-E) \end{aligned} \quad (16)$$

it immediately follows that the CV responses in a cathodic scan and an anodic scan will be symmetric with respect to the point $(E = \bar{E}^0, I_{CV} = 0)$ for any value of ΔE^0 . The conditions in (16) are clearly fulfilled when $k_{1,CV}^0 = k_{2,CV}^0$, that is, when $R_k = 0$ (see Eq. (14) and Fig. 1a).

2 Note that Eq. (16) are also fulfilled in the more general case where $k_{1,CV}^0 \neq k_{2,CV}^0$ (that is, $R_k \neq 0$), if the values of $k_{1,CV}^0$ and $k_{2,CV}^0$ are

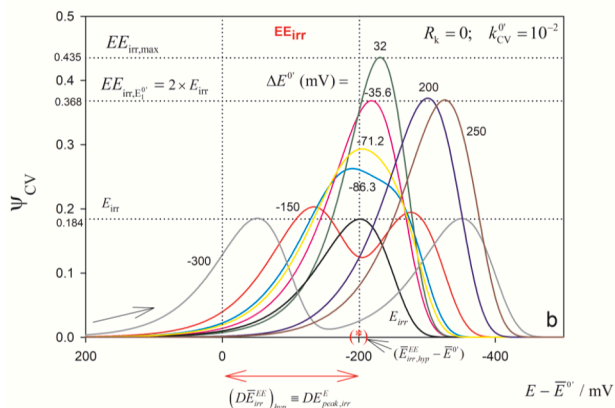
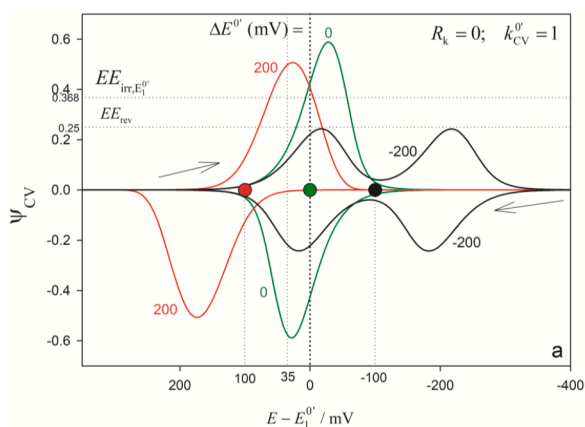


Fig. 1. (a) Dimensionless CV response, $\psi_{CV} - (E - E_1^0)$, for a surface EE process with $R_k = 0$ for $k_{1,CV}^0 = k_{2,CV}^0 (= k_{CV}^0) = 1$, and three values of ΔE^0 (in mV): -200 (black curves, normal ordering of formal potentials), 0 (green curves, transition normal-inverted) and 200 (red curves, inverted ordering of formal potentials) Eqs. (3) and (9). The symmetry point $(\bar{E}^0, 0)$ for each ΔE^0 is marked with a filled circle in the same color as the corresponding CV curve. (b) Forward $\psi_{CV} - (E - E^0)$ curves for the surface EE_{irr} mechanism with $R_k = 0$, $k_{CV}^0 = 10^{-2}$ and several values of ΔE^0 shown on the curves Eqs. (3) and (9). The black curve, $\psi_{CV} - (E - E^0)$, corresponds to an E_{irr} process with $k_{CV}^0 = 10^{-2}$, with E^0 being the formal potential of the redox couple. The point $(\bar{E}_{irr, hyp}^{EE} - E^0, 0)$ is marked with the symbol (*) (see also Eq. (23) for $(D\bar{E}_{irr, hyp}^{EE})$). $\alpha = 0.5$, $T = 298.15$ K.

interchanged between the anodic and the cathodic scans so that Eqs. (14) and (15):

$$R_{k,app,ox} = -R_{k,app,red} \quad (17)$$

Therefore, for any value of ΔE^0 and R_k , the cathodic CV response of a given R_k -value is equivalent to the anodic response of $-R_k$ but rotated 180° around the point $(\bar{E}^0, 0)$ (see Fig. 4b) [23]. This characteristic allows us to easily locate the point $(\bar{E}^0, 0)$ in any experimental response, as indicated in Section 3.2 (see Figure SI-1). Considering such behavior, only reduction or oxidation curves need to be analyzed; hereafter, the study will be focused on the former.

From Eq. (15) with $T = 298.15$ K (see Eq. (8)),

$$R_{k,app,red} = R_k + \frac{1}{118.3} \Delta E^0 \quad (\Delta E^0 \text{ in mV}) \quad (18)$$

$$R_{k,app,ox} = R_k - \frac{1}{118.3} \Delta E^0$$

Note that for $\Delta E^0 = 118.3$ mV, $R_{k,app,red} = R_k + 1$. Thus, a shift of 118.3 mV in ΔE^0 is equivalent to a unity of R_k , i.e. $k_{2,CV}^0 = 10 k_{1,CV}^0$ Eq. (14). For example, from Eq. (18), $R_{k,app,red}$ becomes null for $R_k = 0$ and $\Delta E^0 = 0$, for $R_k = -1$ and $\Delta E^0 = 118.3$ mV, for $R_k = 1$ and $\Delta E^0 = -118.3$ mV, and so on. As will be shown below, some characteristic features of the I/E response are governed by $R_{k,app,red}$ and $R_{k,app,ox}$, therefore being common for the multiple pairs of ΔE^0 and R_k that lead to the same value of these apparent variables. Indeed, Eqs. (15) and (18) point out the complex influence of ΔE^0 in non-reversible EE processes (quasi-reversible – EE_{quasi} – and irreversible – EE_{irr}), in contrast with the case of a reversible behavior (EE_{rev} mechanism) where the role of ΔE^0 is intuitive and well-known: Two well-separated peaks associated to two reversible one-electron transfers appear for $\Delta E^0 \ll 0$ (species I in mechanism (I) is stable) and only one peak corresponding to a reversible two-electron transfer process for $\Delta E^0 \gg 0$ (species I is unstable), with the transition from two peaks to one peak at $\Delta E^0 = -71.2$ mV [13,30]. In contrast, for example, the voltammetry of a non-reversible EE process can show two peaks in the forward scan even for positive values of ΔE^0 , provided that $R_{k,app,red}$ is negative enough, that is, $(k_{1,CV,app}^0)_{red}$ is large enough with respect to $(k_{2,CV,app}^0)_{red}$ (Eq. (15), see Fig. 2b for $R_{k,app,red} < -0.73$, Eq. (18), and Fig. 5); under such conditions, the second ET shows a kinetic hindrance larger than the first ET so that the intermediate species I is 'kinetically stabilized'.

3. Results and discussion

From the definitions and comments in Section 2, it is clear that the CV response of the EE mechanism is controlled by apparent combined parameters Eqs. (13) and (15). Nevertheless, for the sake of practical understanding, results and discussions will be presented in terms of more conventional variables: $k_{1,CV}^0$, $k_{2,CV}^0$, their ratio ($R_k = \log(k_{2,CV}^0/k_{1,CV}^0)$) and $\Delta E^0 (= E_2^0 - E_1^0)$. Simultaneously, the interpretation of the results in terms of the apparent governing variables will be carried out. First, the case where $k_{1,CV}^0 = k_{2,CV}^0$ (that is, $R_k = 0$) will be considered (Section 3.1); next, the generalization to any value of R_k will be carried out (Section 3.2).

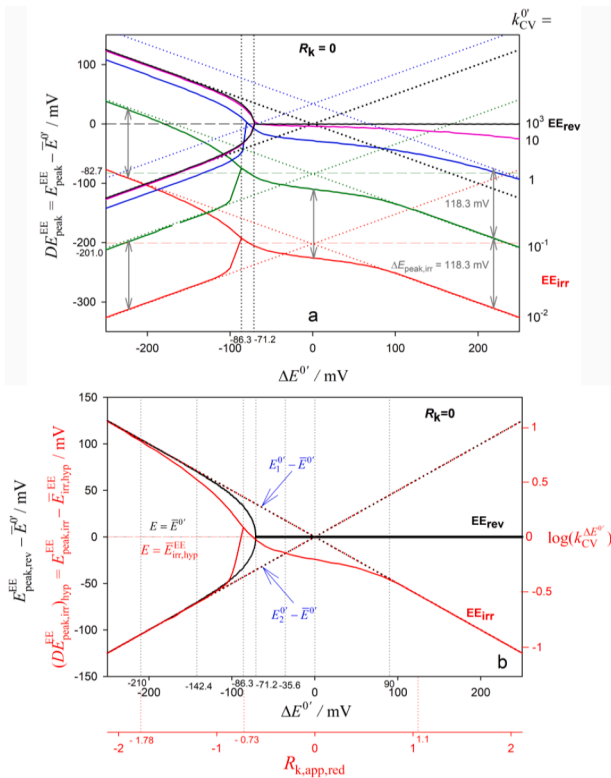


Fig. 2. (a) Solid lines: Evolution of $DE_{peak}^{EE} = (E_{peak}^{EE} - E^0')$ for the forward scan with $\Delta E^0'$ for a surface EE mechanism with $R_k = 0$ and several values of k_{CV}^0 given on the right of the graph: 10^3 (black line) for EE_{rev} behavior; 10 and 1 (magenta and blue lines), transition $EE_{rev} - EE_{quasi}$ and $EE_{quasi} - EE_{irr}$, respectively, as $\Delta E^0'$ increases; 10^{-1} and 10^{-2} (green and red lines), EE_{irr} behavior Eqs. (3) and (9); Dashed green and red lines correspond to $(DE_{irr}^{EE})_{hyp} (= E_{irr,hyp}^{EE} - E^0')$ for $k_{CV}^0 = 10^{-1}$ and 10^{-2} , respectively (Eq. (23)); Dotted lines: $E_i^0' + (DE_{irr}^{EE})_{hyp} - E^0'$ ($i = 1, 2$). The vertical arrow corresponds to a shift of 118.3 mV. b) $R_k = 0$, Left ordinate with upper x-axis: $(DE_{peak,irr}^{EE})_{hyp} (= E_{peak,irr}^{EE} - E_{irr,hyp}^{EE})$ (red line) and $DE_{peak}^{EE} = (E_{peak}^{EE} - E^0')$ (black line) vs $\Delta E^0'$ for EE_{irr} and EE_{rev} surface processes, respectively. Left ordinate with lower red x-axis: $(DE_{peak,irr}^{EE})_{hyp} (= E_{peak,irr}^{EE} - E_{irr,hyp}^{EE})$ (red line) vs $R_{k,app,red}$ for EE_{irr} behavior. Right ordinate, upper x-axis: $\log(k_{CV}^0 \Delta E^0')$ vs $\Delta E^0'$ for EE_{irr} behavior (red line) Eqs. (3), (9) and (30) and (31). Other conditions as in Fig. 1.

3.1. Equal values of the standard heterogeneous rate constants of both ETs ($R_k = 0$)

Fig. 1a shows the dimensionless CV response for a surface EE process with $k_{1,CV}^0 = k_{2,CV}^0 = k_{CV}^0 = 1$ and three values of $\Delta E^0' (= -200 \text{ mV} - \text{normal ordering of the formal potentials}, 0 \text{ mV} - \text{ordering transition} - \text{and } 200 \text{ mV} - \text{inverted ordering})$. In the case under study of $R_k = 0$, as anticipated in Section 2, it can be observed that the response in the reverse scan is morphologically identical to that in the forward scan for all the three values of $\Delta E^0'$, so that voltammograms show a symmetry center at $(E^0', 0)$ [23], which is marked on the graph for each $\Delta E^0'$ -value, i.e., in all cases $R_{k,app,red} = -R_{k,app,ox}$ Eqs. (17) and (18). Hence, only the forward scan will be plotted and discussed in this section. Nevertheless, to locate the point $(E^0', 0)$ in the cyclic experimental response, both scans are to be registered.

As can be seen in Fig. 1a, the reversibility of the EE process for $k_{CV}^0 = 1$ changes depending on $\Delta E^0'$. Indeed, for $\Delta E^0' = -200 \text{ mV}$ (black

curve), the signal shows two peaks with practically reversible behavior ($|\Psi_{CV,peak}| = 0.25$, and the forward and reverse signals being almost symmetrical with respect to the null-current line [30]). When $\Delta E^0'$ increases, the transition from two peaks to one peak is observed, and the forward and reverse signals separate from each other, that is, the process behaves as more irreversible. Indeed, for $\Delta E^0' = 200 \text{ mV}$ (red curve), the dimensionless peak current and the peak position approach the values characteristic of an $EE_{irr,E_1^0'}$ process (0.368 and 35 mV – from Eq. (24) –, respectively, see below). All the above verifies that the variables that act on the reversibility of the CV response are the apparent rate constants given in Eq. (13) (when $R_{k,app,red}$ increases $-R_{k,app,ox}$ decreases –, Eq. (18), the process behaves as more irreversible). Thus, an increase of $\Delta E^0'$ has an effect on the system's reversibility similar to that well-known for a decrease of k_{CV}^0 . Indeed, as k_{CV}^0 decreases, in the EE_{irr} limit, the shape of the CV response for a given $\Delta E^0'$ -value becomes independent of k_{CV}^0 (see Fig. 1b), which only affects the position of the signal: the smaller the k_{CV}^0 -value, the more negative (or positive) the position of the cathodic (or anodic) response (so that the separation between the forward and reverse responses increases, see Fig. 2a), while

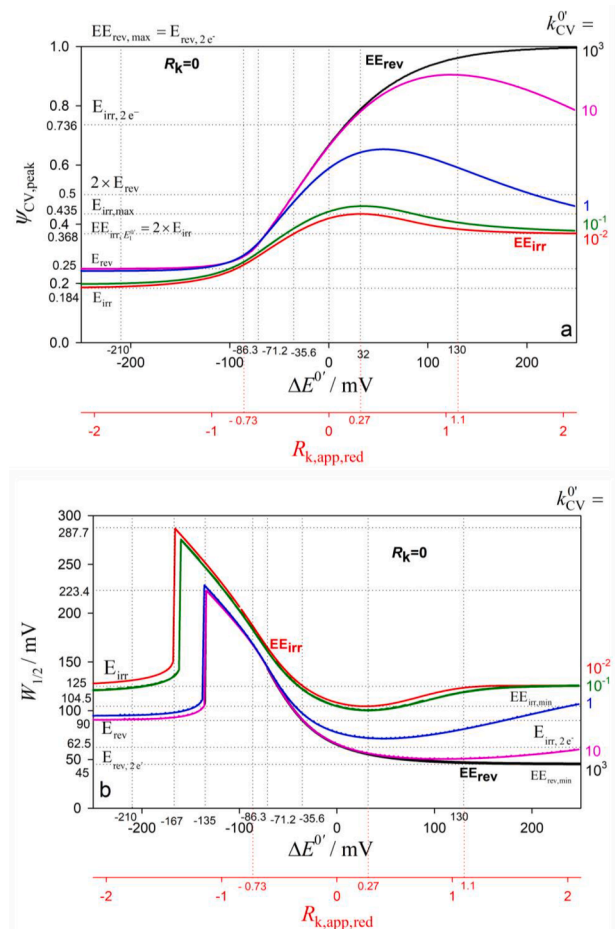


Fig. 3. Upper x-axis: Evolution with $\Delta E^0'$ of the dimensionless peak height, $\Psi_{CV,peak}$ Fig. 3a, for the forward scan), and the half-peak width, $W_{1/2}$ (Fig. 3b) for a surface EE mechanism with $R_k = 0$ for different values of k_{CV}^0 , shown in the figure: 10^3 (black line) for EE_{rev} behavior; 10 and 1 (magenta and blue lines), transition $EE_{rev} - EE_{quasi}$ as $\Delta E^0'$ increases; 10^{-1} and 10^{-2} (green and red lines), nearly EE_{irr} and EE_{irr} behaviors, respectively (Eqs. (3) and (9)). Lower x-axis for EE_{irr} behavior (red curve): $\Psi_{CV,peak}$ (Fig. 3a) and $W_{1/2}$ (Fig. 3b) vs $R_{k,app,red}$. When two peaks appear in the $I-E$ signal, $\Psi_{CV,peak}$ and $W_{1/2}$ refer to the first one. Other conditions as in Fig. 1.

the peak height and width are unaffected (see red lines in Fig. 3a and b).

Fig. 1b shows the forward $\psi_{CV} - (E - \bar{E}^0)$ curves for a surface EE_{irr} mechanism with $k_{CV}^0 = 10^{-2}$ and several distinctive values of ΔE^0 . The curve corresponding to a single irreversible ET (E_{irr} mechanism) with $k_{CV}^0 = 10^{-2}$ [16] has also been included as a reference (solid black curve, $\psi_{CV} - (E - E^0)$ with E^0 being the formal potential of the redox couple). As can be observed, two well-separated, identical peaks are obtained for very negative values of ΔE^0 (see gray curve). As ΔE^0 increases, the two peaks gradually approach, the first one being slightly larger than the second one (see red curve); subsequently, the peaks merge together for $\Delta E^0 \geq -86.3$ mV (see light blue curve and Figs. 2a and b), with the peak height increasing with ΔE^0 and the peak potential shifting towards more negative values vs \bar{E}^0 . In this single-peak regime, some characteristic ΔE^0 -values can be highlighted:

- $\Delta E^0 = -71.2$ mV (yellow curve, transition from two peaks to one peak for an EE_{rev} [30]): The position of the peak in the EE_{irr} process (vs \bar{E}^0) is practically the same as that for an E_{irr} process (vs E^0) -see the abscissa labelled with (*).
- $\Delta E^0 = -35.6$ mV (magenta curve): The peak height of an EE_{irr} is double that of an E_{irr} , as occurs for the EE_{rev} mechanism with respect to the E_{rev} mechanism (i.e., a single reversible ET) [30].
- $\Delta E^0 \simeq 32$ mV (green curve): The maximum peak height of EE_{irr} is attained (for $R_{k,app,red} = 0.27$, Eq. (18), see Figs. 3a and b with the lower x-axis).
- Further increase of ΔE^0 leads to the decrease of the peak current, which eventually reaches again a value that doubles that of E_{irr} (see dark blue and brown curves for $\Delta E^0 = 200$ and 250 mV, respectively). Indeed, the I/E curves become independent of ΔE^0 and identical to that for $\Delta E^0 = -35.6$ mV, only shifted towards more negative potentials with respect to \bar{E}^0 , but always situated at the corresponding E_1^0 , displaced by a quantity dependent on k_{CV}^0 (see below and Fig. 2b). This limiting situation, dominated by the first ET, where ΔE^0 only affects the position of the peak, has been here referred to as EE_{irr,E_1^0} , and it is attained for $\Delta E^0 > 130$ mV (less than 5% difference in peak current and than 2 mV difference in the half-peak width), that is, for $R_{k,app,red} > 1.1$ (Eq. (18), see Figs. 3a and b with the lower x-axis).

In Fig. 2a, the difference between the peak potentials predicted for the EE mechanism for the forward scan, E_{peak}^{EE} , and the average formal potential, \bar{E}^0 , are plotted versus ΔE^0 for several values of k_{CV}^0 (given on the figure):

$$DE_{peak}^{EE} = E_{peak}^{EE} - \bar{E}^0 \quad (19)$$

where both E_{peak}^{EE} and \bar{E}^0 can be directly obtained from the experimental response. Note that, depending on the k_{CV}^0 values, different behaviors are found:

- EE_{rev} mechanism:

For $k_{CV}^0 = 10^3$ (solid black line), the behavior of the EE_{rev} mechanism is recognized, the $I-E$ signal showing a single peak at \bar{E}^0 (dashed black line) for $\Delta E^0 \geq -71.2$ mV and two peaks equidistant from \bar{E}^0 for $\Delta E^0 < -71.2$ mV. Note that for $\Delta E^0 \leq -142.4$ mV (see Fig. 2b) [30], the peak potentials coincide with the respective formal potentials, so that the

solid black lines in Fig. 2a overlap with the dotted black straight lines with slope $-1/2$ and $1/2$, corresponding to the plots $E_1^0 - \bar{E}^0$ and $E_2^0 - \bar{E}^0$ vs ΔE^0 , respectively, according to Eqs. (1) and (2),

$$E_i^0 = \bar{E}^0 \mp \frac{\Delta E^0}{2} \quad i = 1, 2 \quad (20)$$

- EE_{irr} mechanism:

With regard to the EE_{irr} mechanism, in terms of peak position(s) this limit holds for $k_{CV}^0 < 10^{-1} \sim k_{CV}^0 \lesssim 10^{-1}$ (red and green lines in Fig. 2a). In the EE_{irr} regime, the transition from one to two peaks takes place around $\Delta E^0 = -86.3$ mV. Regardless of the ΔE^0 -value, the peak potential(s) show(s) a characteristic shift of 118.3 mV ($\simeq 120$ mV) per decade of k_{CV}^0 (at $T = 298.15$ K, compare red and green curves in Fig. 2a),

$$\begin{aligned} (DE_{peak,irr})_{any \Delta E^0} &= E_{peak,irr,i}^{EE}(at k_{CV}^0) - E_{peak,irr,i}^{EE}(at 0.1k_{CV}^0) \\ &= 118.3 \text{ mV} \quad (i = 1 \text{ or } 2) \end{aligned} \quad (21)$$

This shift of the peak potential with k_{CV}^0 is equivalent to that predicted by the Laviron equation for an E_{irr} mechanism, which for $\alpha = 0.5$ fulfills that [16]:

$$DE_{peak,irr}^E = E_{peak,irr}^E - E^0 = 35.6 + 118.3 \log k_{CV}^0 \quad (\text{in mV}) \quad (22)$$

The $DE_{peak,irr}^E$ -value quantifies the shift of the peak potential of an E_{irr} process with respect to an E_{rev} reaction (for which $E_{peak,rev}^E = E^0$) as a function of the standard heterogeneous rate constant, k_{CV}^0 , which is -201.0 mV for $k_{CV}^0 = 10^{-2}$ (marked under the abscissa axis of Fig. 1b). Analogously, in the EE_{irr} case, taking this time as reference the average formal potential, \bar{E}^0 , around which the EE_{rev} signal is centered (see Fig. 2), and attending to the influence of k_{CV}^0 , one can conveniently introduce a hypothetical average potential, $\bar{E}_{irr,hyp}^{EE}$, by supposing that this is shifted from \bar{E}^0 in a quantity identical to $DE_{peak,irr}^E$ in Eq. (22). Such quantity for EE_{irr} is referred to as $(DE_{irr,hyp}^{EE})$ and it is therefore defined as (see under the abscissa axis in Fig. 1b):

$$(DE_{irr,hyp}^{EE}) = \bar{E}_{irr,hyp}^{EE} - \bar{E}^0 = 35.6 + 118.3 \log k_{CV}^0 \quad (\text{in mV}) \quad (23)$$

The point $(\bar{E}_{irr,hyp}^{EE} - \bar{E}^0, 0)$ is marked as (*) in Fig. 1b. Also, in Fig. 2a, the $(DE_{irr,hyp}^{EE})$ values for $k_{CV}^0 = 10^{-1}$ and $k_{CV}^0 = 10^{-2}$ have been indicated as dashed horizontal straight green and red lines, respectively, which are separated by -82.7 mV and -201.0 mV, respectively, from the dashed horizontal straight black line corresponding to $E_{peak}^{EE} = \bar{E}^0$ (see the ordinate axis in Fig. 2a). Note that these same values separate the dotted green and red straight lines (with slope $\pm 1/2$), respectively, from the corresponding dotted black lines. Therefore, it is important to highlight that, in the range of values of ΔE^0 where the dotted lines overlap with their corresponding solid ones, the peak of the EE_{irr} is located at $E_1^0 + (DE_{irr,hyp}^{EE})_{hyp}$ (negative slope) or at $E_2^0 + (DE_{irr,hyp}^{EE})_{hyp}$ (positive slope). Thus, the position of the peaks is the same as that of an E_{irr} mechanism of formal potential E_i^0 ($i = 1, 2$), i.e. (see Eq. (22)),

$$E_{peak,irr}^{EE} = E_i^0 + 35.6 + 118.3 \log k_{CV}^0 \quad (\text{in mV}) \quad (i = 1, 2) \quad (24)$$

- The quasireversible transition (EE_{quasi})

For intermediate values of k_{CV}^0 (see solid magenta and blue lines for $k_{CV}^0 = 10$ and 1, respectively, in Fig. 2a), it can also be observed that the peak potentials correspond to a process that behaves more irreversibly as ΔE^0 increases. Indeed, for $k_{CV}^0 = 10$ a clear evolution from the EE_{rev} to the EE_{quasi} behavior is observed (the solid magenta line separates from the reversible black one for $\Delta E^0 > -50$ mV for differences larger than 2 mV), whereas for $k_{CV}^0 = 1$, a EE_{quasi} to EE_{irr} transition can be seen (for $\Delta E^0 > 250$ mV solid and dotted blue lines are coincident, indicating an irreversible behavior).

Note that the value of ΔE^0 for which the transition two peaks-one peak takes place is scarcely affected by the reversibility of the process for $R_k = 0$ (just ≈ 15 mV), being slightly more negative for an EE_{irr} process ($\Delta E^0 = -86.3$ mV, corresponding to $R_{k,app,red} = -0.73$, Eq. (18), see Fig. 2b with the lower x-axis) than for an EE_{rev} one ($\Delta E^0 = -71.2$ mV).

The quantitative kinetic analysis of the EE_{quasi} regime is obviously more awkward than the EE_{irr} limit. Attending to that the k_{CV}^0 -value decreases when the scan rate is increased Eqs. (10) and (11), the experimental scan rate can be suitably adjusted in order to reach the EE_{irr} behavior. Note that in such strategy the minimization or compensation of ohmic drop effects is to be considered since their influence on the CV response (broader and smaller peaks, larger peak-to-peak separation) can be misinterpreted as kinetic limitations of the ETs. Nevertheless, for a large number of experimental systems, the values of scan rate required to reach the EE_{irr} behavior are not too high (typically in the range of $1 - 10$ V s⁻¹).

3.1.1. Determination of k_{CV}^0

In order to obtain the value of k_{CV}^0 for an EE_{irr} process, in Fig. 2b (see red line) $DE_{peak,irr}^{EE} - (DE_{irr}^{EE})_{hyp} (= E_{peak,irr}^{EE} - E_{irr,hyp}^{EE})$ has been plotted versus ΔE^0 (upper x-axis) Eqs. (19) and (23), i.e., $(DE_{peak,irr}^{EE})_{hyp}$ vs ΔE^0 with:

$$\left(DE_{peak,irr}^{EE} \right)_{hyp} = E_{peak,irr}^{EE} - E_{irr,hyp}^{EE} \quad (25)$$

The lower x-axis will be discussed for any R_k in Section 3.2. Note that the solid black line in Fig. 2b for the surface EE_{rev} mechanism ($DE_{peak,rev}^{EE} = E_{peak,rev}^{EE} - E^0$, Eq. (19)) has also been added (as in Fig. 2a). According with the above discussion for Figs. 1 and 2a, Fig. 2b is valid for an EE_{irr} process with any $k_{CV}^0 < 10^{-1}$ Eq. (23). Under these conditions, the value of k_{CV}^0 can be determined from Fig. 2b, if the value of ΔE^0 is known (see below for the determination of ΔE^0). Thus, the value of $(DE_{peak,irr}^{EE})_{hyp}$ can be obtained as the left ordinate (in mV) of the red curve at the corresponding ΔE^0 -value and then the k_{CV}^0 -value can be extracted from the following general expression (Eqs. (19), (23) and (25)):

$$\log k_{CV}^0 = \frac{E_{peak,irr}^{EE} - E^0 - (DE_{peak,irr}^{EE})_{hyp} - 35.6 \text{ (in mV)}}{118.3} \quad (26)$$

So, from Eq. (26) the value of k_{CV}^0 can be obtained from the experimental I/E response and Fig. 2b. When two peaks are obtained, this calculation can be done twice (see also Section 3.1.3).

The above procedure is valid for any value of ΔE^0 . Nevertheless, as explained above, in the particular case where the red line in Fig. 2b is coincident with the dotted straight lines with slope $-1/2$ (for $\Delta E^0 < -210$ mV and $\Delta E^0 > 90$ mV), and $1/2$ (for $\Delta E^0 < -110$ mV and $\Delta E^0 = -35.6$ mV), the value of k_{CV}^0 can be obtained directly from the experimental I/E response and using Eq. (24). Note that, according to Eq. (20), the formal potentials E_i^0 ($i = 1, 2$) are known from the values of E^0

(obtained experimentally) and ΔE^0 (determined as indicated in Section 3.1.2). Alternatively, taking into account Eq. (20), from Eq. (24) it is obtained that,

$$\log k_{CV}^0 = \frac{E_{peak,irr}^{EE} - E^0 - \left(\mp \frac{\Delta E^0}{2} \right) - 35.6 \text{ (in mV)}}{118.3} \quad (27)$$

where the signs (-) and (+) in the ΔE^0 -term refer to the sign of the slope of the dotted lines. Thus, for the values of ΔE^0 fulfilling Eq. (27) (see Fig. 2b), the value of k_{CV}^0 can be obtained directly from the experimental I/E response and using Eq. (27) (see also Section 3.1.3).

3.1.2. Determination of ΔE^0 and Γ_T

The value of ΔE^0 , when two peaks appear in the voltammogram of an EE_{irr} process, can be directly obtained from the difference $\Delta E_{peak} = (E_{peak,irr,2}^{EE} - E_{peak,irr,1}^{EE})$ and Fig. 2b. Also, for any value of ΔE^0 , Fig. 3 can be used.

Figs. 3a and b show the evolution with ΔE^0 (upper x-axis) of the dimensionless peak height, $\psi_{CV,peak}$, and the half-peak width, $W_{1/2}$, respectively, for a surface EE mechanism with different values of k_{CV}^0 (shown in the figure) that cover from the EE_{rev} (black line) to the EE_{irr} (red line) behaviours, going through the quasireversible transition. The lower x-axis will be discussed in Section 3.2 for any R_k value. Note that the values of peak height and half-peak width reach the EE_{irr} limit (red line) at smaller k_{CV}^0 than the peak potential; indeed, for $k_{CV}^0 = 10^{-1}$, where the peak potential behaves as in the EE_{irr} case (Fig. 2a), the peak is still larger (Fig. 3a) and sharper (Fig. 3b) than the EE_{irr} peak (compare green and red lines).

As can be observed in Fig. 3b, $W_{1/2}$ for EE_{irr} is very sensitive to the ΔE^0 value in the interval -167 mV $< \Delta E^0 < -35.6$ mV, whereas two possible values of ΔE^0 are obtained in the interval -35.6 mV $< \Delta E^0 < 130$ mV (for 2 mV-difference in $W_{1/2}$). In this case, the scan rate can be decreased in order to reach the EE_{rev} behavior and obtain ΔE^0 from the black curve in Fig. 3b. For $\Delta E^0 \geq 130$ mV the I/E response is identical for any value of ΔE^0 , only its position in the E-axis changing (see Fig. 1b), and the value of ΔE^0 cannot be discriminated. Therefore, the value of k_{CV}^0 cannot be extracted (the position of the peak would lead to infinite couples $k_{CV}^0 - \Delta E^0$). In this case, corresponding to EE_{irr,E_1^0} (Fig. 1b), only the global combined influence of k_{CV}^0 and ΔE^0 on the irreversibility can be evaluated from the experimental data (see Section 3.1.3).

Alternatively, $\psi_{CV,peak}$ in Fig. 3a can be used for $\Delta E^0 < 130$ mV (differences larger than 5% in peak current) to determine the ΔE^0 value if the total surface coverage, Γ_T , is known Eqs. (6) and (9). Conversely, if ΔE^0 is known, Γ_T can be determined from Fig. 3a.

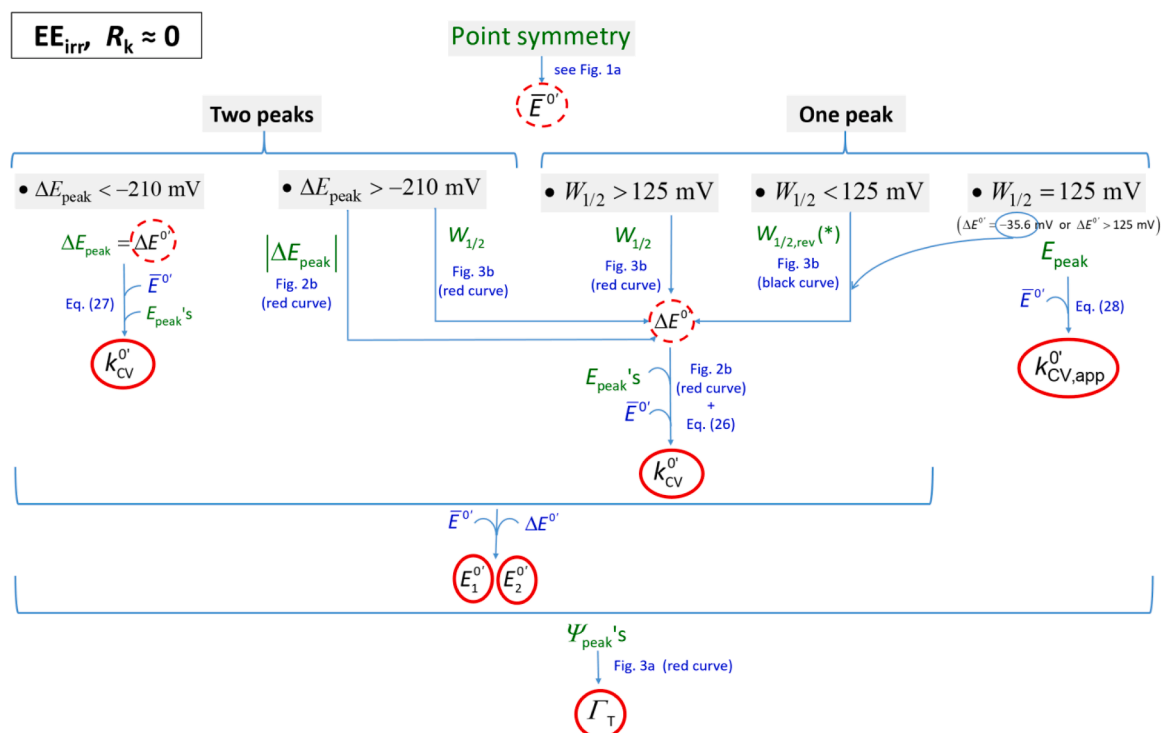
In order to guide the experimental kinetic analysis of the EE_{irr} mechanism with $R_k \approx 0$, the above results have been summarized in Scheme 1.

3.1.3. Considerations about the EE_{irr} behavior. Comparison with the EE_{rev} mechanism

From Eq. (26), the expression of the peak potentials for an EE_{irr} process can be written in the following form, in a parallel manner to that for an EE_{irr} (Eq. (22)),¹

$$E_{peak,irr}^{EE} - E^0 = 35.6 + 118.3 \log k_{CV,app}^0 \text{ (in mV)} \quad (28)$$

¹ In this section, the subscript "red" for the apparent rate constants will be omitted for the sake of simplicity.



Scheme 1. Flowchart of the protocol proposed for the determination of the heterogeneous rate constant and the formal potentials of the two ETs from the key features of the experimental CV signal of an EE_{irr} mechanism for the case $R_k \approx 0$, with $\alpha = 0.5$ and $T = 298.15$ K.

(*) When one peak is obtained with $W_{1/2} < 125$ mV, two possible values of $\Delta E^{0'}$ are compatible with the experimental peak (see Fig. 3b), except for $W_{1/2} = 104.5$ mV that corresponds to $\Delta E^{0'} = 32$ mV. To discriminate between them, an independent determination of $\Delta E^{0'}$ is necessary, for example, by decreasing the scan rate so that the EE_{rev} regime is approached and the $\Delta E^{0'}$ -value can be unambiguously determined from $W_{1/2,rev}$ (black curve in Fig. 3b).

with $k_{CV,app}^{0'}$ being an apparent rate constant that accounts for the influence of the kinetics and thermodynamics of both ET processes on the global rate, defined as,

$$k_{CV,app}^{0'} = k_{CV}^{0'} k_{CV}^{\Delta E^{0'}} \quad (29)$$

where $k_{CV}^{\Delta E^{0'}}$ is given by

$$k_{CV}^{\Delta E^{0'}} = 10^{\frac{(DE_{peak,irr}^{EE})_{hyp}}{118.3}} \quad (\text{in mV}) \quad (30)$$

with $(DE_{peak,irr}^{EE})_{hyp}$ referring to the left ordinate (in mV) of the red curve at the corresponding $\Delta E^{0'}$ -value in Fig. 2b. For the values of $\Delta E^{0'}$ for which Eq. (27) is fulfilled, it holds that $(DE_{peak,irr}^{EE})_{hyp} = \mp \Delta E^{0'}/2$ and $k_{CV}^{\Delta E^{0'}}$ becomes into (see Eq. (13))

$$k_{CV}^{\Delta E^{0'}} = 10^{\frac{\mp \Delta E^{0'}}{118.3}} = e^{\mp \frac{\Delta E^{0'}}{2}} \quad (31)$$

In any case, the $k_{CV}^{\Delta E^{0'}}$ -value represents the contribution of $\Delta E^{0'}$ to the apparent rate constant (see the right ordinate axis in Fig. 2b), which can have a significant effect on the apparent kinetics; for example, for $\Delta E^{0'} = 118.3$ mV, Eq. (31) with the negative sign yields $k_{CV}^{\Delta E^{0'}} = 0.32$, i.e. $k_{CV}^{0'} = 3.13 k_{CV,app}^{0'}$.

Note that Eq. (28) is formally similar to the Laviron equation for an E_{irr} mechanism Eq. (22) but in terms of $k_{CV,app}^{0'}$ of the EE_{irr} process so that $k_{CV,app}^{0'}$ can be easily obtained via a data analysis equivalent to that proposed by Laviron [16]. Thus, if $\Delta E^{0'}$ is accessible and so $k_{CV}^{\Delta E^{0'}}$ (Eq.

(30) or ((31), Fig. 2b), the $k_{CV}^{0'}$ -value can be immediately obtained (Eq. (29)).

The following characteristic cases for an EE_{irr} mechanism can be considered:

1 For values of $\Delta E^{0'}$ fulfilling Eq. (27) ($k_{CV,app}^{0'} = k_{i,CV,app}^{0'} - i = 1, 2$), the position of the peaks is the same as that for an E_{irr} mechanism with formal potential $E_i^{0'}$ ($i = 1, 2$, see Eqs. (22) and (24)).

a) $\Delta E^{0'} \ll 0$ (normal ordering of formal potentials). From Eq. (13), $k_{1,CV,app}^{0'} \gg k_{2,CV,app}^{0'}$ ($R_{k,app,red} \ll 0$, Eq. ((18))) and two well-separated peaks are obtained, each one corresponding to an E_{irr} process with the two peak potentials being given by $E_{peak,irr,i}^E = E_i^{0'} + DE_{peak,irr}^E$ ($i = 1, 2$) (Eq. (22), Figs. 1–3). Since $E_{peak,rev,i}^E = E_i^{0'}$ ($i = 1, 2$) the separation between the peaks is the same as that for two E_{rev} processes (see Fig. 2b for $\Delta E^{0'} \leq -210$ mV, $R_{k,app,red} \leq -1.78$).

b) $\Delta E^{0'} = -35.6$ mV. From Eq. (13), $k_{1,CV,app}^{0'} = 2 k_{2,CV,app}^{0'}$ ($R_{k,app,red} < 0$,

Eq. (18)). The peak obtained is situated at $E_{peak,irr}^{EE} = E_2^{0'} + (DE_{irr}^{EE})_{hyp}$ ($k_{CV,app}^{0'} = k_{2,CV,app}^{0'} = 0.71 k_{CV}^{0'}$) (see Fig. 2b). This value of $\Delta E^{0'}$ gives rise to an I/E response that is double that of an E_{irr} process, as in the case of an EE_{rev} mechanism in relation to an E_{rev} process [30] (see Figs. 1b and 3), and even for quasireversible ETs this is so with ca. 3% difference (see Fig. SI-2a). In this particular case of $\Delta E^{0'} = -35.6$ mV, it is fulfilled that the surface coverages of species O, I and R in reaction scheme (1) show characteristic relationships that hold independently of the reversibility degree of the ETs (see Fig. SI-2b in SI).

c) $\Delta E^0 \gg 0$ (inverted ordering of formal potentials). From Eq. (13), $k_{1,CV,app}^0 \ll k_{2,CV,app}^0$ ($R_{k,app,red} \gg 0$, Eq. ((18))), and the first ET determines the rate of the overall process ($k_{CV,app}^0 = k_{1,CV,app}^0$). The intermediate species I in mechanism (I) is unstable and only one peak is obtained, being $E_{peak,irr}^{EE} = E_1^0 + (DE_{irr}^{EE})_{hyp}$. Thus, the peak potential varies linearly with ΔE^0 (see Fig. 2b for $\Delta E^0 > 90$ mV), i.e. with $\log k_{CV}^0$ Eqs. (27) and (31), see the right ordinate axis in Fig. 2b, moving to more negative values (vs \bar{E}^0) as ΔE^0 increases (see Eqs. (29) and (31)). As discussed above, for $\Delta E^0 > 130$ mV only $k_{CV,app}^0$ can be obtained from the experimental response. In this limit EE_{irr,E_1^0} situation, the I/E signal is double that of an E_{irr} (and morphologically identical to that for $\Delta E^0 = -35.6$ mV, see Figs. 1b and 3). In the case EE_{rev} , as it is seen in Figs. 2 and 3, in this limit of $\Delta E^0 \gg 0$ the behavior of a two-electron E_{rev} mechanism is attained, with $E_{peak,rev}^{EE} = \bar{E}^0$ [30]. This limit (two-electron E_{irr}) is not reached for an EE_{irr} (see Fig 3 [7]).

2 For values of ΔE^0 not fulfilling Eq. (27), there is a mixed control of the overall rate of the process by $k_{1,CV,app}^0$ and $k_{2,CV,app}^0$, which is parameterized by $k_{CV,app}^0$.

a) -86.3 mV $\leq \Delta E^0 \leq -71.2$ mV ($R_{k,app,red} < 0$, Eq. ((18))). In this short ΔE^0 -range, there is a peculiar behavior of the EE_{irr} mechanism, which shows a single peak (unlike EE_{rev}) situated at more positive potentials than $(\bar{E}_{irr}^{EE})_{hyp}$ ($(DE_{peak,irr}^{EE})_{hyp} > 0$) so that $k_{CV,app}^0 > k_{CV}^0$ Eqs. (29) and (30). For $\Delta E^0 \approx -71.2$ mV, it holds that $(DE_{peak,irr}^{EE})_{hyp} = 0$ (i.e., $E_{peak,irr}^{EE} = \bar{E}_{irr,hyp}^{EE}$) so that $k_{CV,app}^0 = k_{CV}^0$ (see Fig. 1b).

b) -71.2 mV $< \Delta E^0 \leq 90$ mV: the EE_{irr} I/E response shows a single peak at more negative potentials than $\bar{E}_{irr,hyp}^{EE}$ ($(DE_{peak,irr}^{EE})_{hyp} < 0$) so that $k_{CV,app}^0 < k_{CV}^0$.

In the particular case $\Delta E^0 = 0$ (transition between the normal and inverted ordering of formal potentials) where $k_{1,CV,app}^0 = k_{2,CV,app}^0 = k_{CV}^0$ ($R_{k,app,red} = 0$, Eq. ((18))), there is an inflexion point in the red curve in Fig. 2b and $k_{CV,app}^0 = 0.63 k_{CV}^0$.

3.2. Different values of the heterogeneous rate constants of both ETs ($R_k = \log(k_{2,CV}^0/k_{1,CV}^0) \neq 0$)

The previous discussion of the EE mechanism for $R_k = 0$ in Section 3.1 can be used as a reference to describe the general behavior of an EE process for different values of $k_{1,CV}^0$ and $k_{2,CV}^0$ ($R_k \neq 0$).

In Fig. 4a it is plotted the dimensionless CV curves for the transition ΔE^0 -value between the normal and inverted ordering of formal potentials, $\Delta E^0 = 0$ mV (for which a single peak is observed for an EE_{rev} process [30]), and $k_{2,CV}^0/k_{1,CV}^0 = 0.1$ ($R_k = -1$) at different values of $k_{1,CV}^0$, which can be varied conveniently through the change of the scan rate. As can be seen, the CV curves obtained transit through the following behaviors as the scan rate is decreased (see also Figure SI-3):

- A practically EE_{irr} behavior ($k_{1,CV}^0 = 10^{-1}$, $k_{2,CV}^0 = 10^{-2}$, blue curve), with the forward and reverse scans showing two and one peaks, respectively.

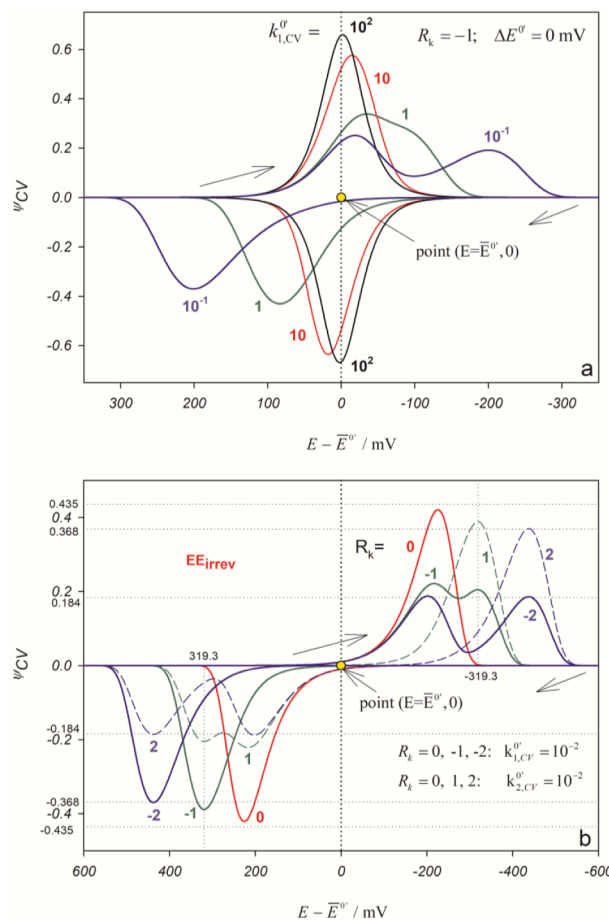


Fig. 4. a) Dimensionless CV response, $\psi_{CV} - (E - \bar{E}^0)$, for a surface EE process with $R_k = -1$, $\Delta E^0 = 0$ mV (transition normal-inverted ordering of formal potentials) and several values of $k_{1,CV}^0$: 10^2 (black curves, $k_{2,CV}^0 = 10$, practically EE_{rev} behavior); 10 (red curves, $k_{2,CV}^0 = 1$, EE_{quasi} behavior); 1 (green curves, $k_{2,CV}^0 = 10^{-1}$, EE_{quasi} behavior); 10^{-1} (blue curves, $k_{2,CV}^0 = 10^{-2}$, practically EE_{irr} behavior) Eqs. (3) and (9). The point ($E = \bar{E}^0$, 0) is marked with a filled yellow circle. b) Dimensionless CV response, $\psi_{CV} - (E - \bar{E}^0)$, for a surface EE_{irr} mechanism with $\Delta E^0 = 0$ mV at several values of R_k , shown on the curves: 0 (red curves, $k_{1,CV}^0 = k_{2,CV}^0 = 10^{-2}$); -1 (solid green curves, $k_{1,CV}^0 = 10^{-2}$, $k_{2,CV}^0 = 10^{-3}$); -2 (solid blue curves, $k_{1,CV}^0 = 10^{-2}$, $k_{2,CV}^0 = 10^{-4}$); 1 (dashed green curves, $k_{1,CV}^0 = 10^{-3}$, $k_{2,CV}^0 = 10^{-2}$); 2 (dashed blue curves, $k_{1,CV}^0 = 10^{-4}$, $k_{2,CV}^0 = 10^{-2}$). The point ($E = \bar{E}^0$, 0) is marked with a filled yellow circle. Other conditions as in Fig. 1.

- An EE_{quasi} behavior. For $k_{1,CV}^0 = 1$, $k_{2,CV}^0 = 10^{-1}$ (green curve), two partially overlapped peaks are observed in the forward scan and a single peak in the reverse one, so that the reduction and oxidation signals are still asymmetric. As $k_{1,CV}^0$ is increased ($k_{1,CV}^0 = 10$, $k_{2,CV}^0 = 1$, red curve), the two peaks of the forward response merge into one that is almost symmetric to the peak in the reverse response.
- A practically EE_{rev} behavior ($k_{1,CV}^0 = 10^2$, $k_{2,CV}^0 = 10$, black curve) with the CV response being practically symmetric [30].

Fig. 4b shows the dimensionless CV response of an EE_{irr} with $\Delta E^0 = 0$ mV and several values of R_k ($= -2, -1, 0, 1, 2$). As can be observed, for any value of $R_k \neq 0$ and regardless of the values of the rate constants of the ETs, the responses for the forward and reverse scans are different.

the top of Fig. 5).

Figs. 3a and 3b (red lines) with the lower x-axis show the evolution of the dimensionless peak height, $\psi_{CV,peak}$, and the half-peak width, $W_{1/2}$, respectively, with $R_{k,app,red}$. These curves for the EE_{irr} behavior are independent of the particular values of $k_{1,CV}^0$ and $k_{2,CV}^0$. From Fig. 5 it can be seen, for example, that for $\Delta E^0 = 0$ and $R_k = -2$ ($R_{k,app,red} = -2$, Eq. (18)) (solid blue curve), two peaks very separated are obtained, the height (Fig. 3a, red line) and $W_{1/2}$ (Fig. Fig. 3b, red line) of which are coincident with those of an E_{irr} process. This behavior as two separated E_{irr} processes is the same as that for $R_k = 0$ and $\Delta E^0 = -236.6$ mV and of any other combination of R_k and ΔE^0 yielding $R_{k,app,red} = -2$.

3.2.1. Determination of characteristic parameters

Taking into account the variety of parameters that influence the I/E response of an EE_{irr} process, and according with the previous discussions, when $R_k \neq 0$, that is, the forward and reverse signals are different, the value of ΔE^0 (and \bar{E}^0) can be obtained by decreasing the scan rate in order to reach the EE_{rev} behavior (see Figs. 4a and SI-3) and using Fig. 3 for a EE_{rev} mechanism (black lines, see Section 3.1.2). Parallely, the $R_{k,app,red}$ -value can be extracted from $W_{1/2}$ (red line in Fig. 3b with lower x-axis) or from the peak-to-peak separation when two peaks are observed (red line in Fig. 2b with lower x-axis). Then, the R_k -value can be immediately obtained from ΔE^0 and $R_{k,app,red}$ and, finally, the peak potential(s) enable us to determine the individual values of the rate constants (red line in Fig. 2b with lower x-axis). These results are summarized in Scheme 2.

4. Conclusions

The CV of the surface non-reversible EE mechanism has been unraveled, for any degree of reversibility and any ordering of the formal potentials, through the introduction of the apparent rate constants ($k_{1,CV,app}^0$)_{red/ox} and ($k_{2,CV,app}^0$)_{red/ox} that account for the combined influences of the standard heterogeneous rate constants, the formal potentials and the scan rate. The individual values of ($k_{1,CV,app}^0$)_{red/ox} and ($k_{2,CV,app}^0$)_{red/ox} and of their ratio (through the combined parameters

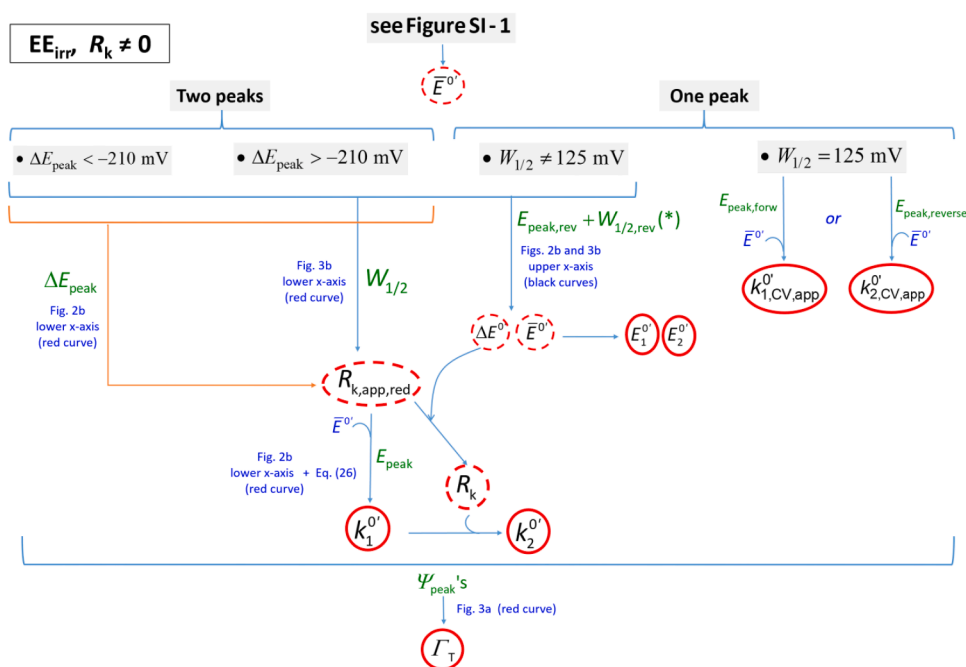
$R_{k,app,red}$ and $R_{k,app,ox}$) have been demonstrated to govern the variety of patterns and behaviors of the CV response, so that both the kinetics and the thermodynamics of the ETs are to be considered simultaneously in the data analysis to avoid misinterpretations.

Although the quasireversible regime shows the most complex and parametrized CV response, general behaviors have been discussed as a function of the apparent rate constants. Thus, when the values of the heterogeneous rate constants are similar, regardless of the reversibility degrees, the cyclic voltammograms show a symmetry center at the zero-current axis situated at the average formal potential. On the other hand, the situation where the heterogeneous rate constants differ notably can be detected by different features (sometimes including different number of peaks) of the signal obtained in the forward and the reverse scans.

For an accurate quantitative analysis, it is convenient to reach the irreversible behavior (EE_{irr}) in order to facilitate the quantitative kinetic analysis. Note that varying the experimental scan rate enables us to modulate the kinetic regime of the system at convenience. Once in the EE_{irr} regime, the features of the response (number of peaks, peak height, half-peak width and peak-to-peak separation) are only a function of the corresponding $R_{k,app,red/ox} = \log(k_{2,CV,app}^0/k_{1,CV,app}^0)_{red/ox} = R_k \pm \frac{0.5f}{2.3} \Delta E^0$, independently of the particular values of $k_{1,CV}^0$ and $k_{2,CV}^0$. In the particular case of $k_{1,CV}^0 = k_{2,CV}^0$, the definition of a new $k_{CV,app}^0$ Eqs. (29)–(31) allows us to express the peak potentials for an EE_{irr} in a similar way to that for an E_{irr} mechanism.

Simple protocols of quantitative analysis have been established on the basis of simple mathematical relationships and/or working curves for the peak potential(s), the dimensionless peak height and the half-peak width versus ΔE^0 and $R_{k,app,red/ox}$, from which the values of k_{CV}^0 (similar heterogeneous rate constants) or $k_{1,CV}^0$ and $k_{2,CV}^0$ (different heterogeneous rate constants), ΔE^0 and Γ_T can be extracted for $\Delta E^0 < 130$ mV; otherwise, the kinetic and thermodynamic contributions to $k_{CV,app}^0$ cannot be discriminated since the behavior controlled by the first transfer is achieved where it is possible to quantify their combined influence but not their individual values.

To sum up, the behavior of the EE process is more irreversible as the $k_{1,CV}^0$ and $k_{2,CV}^0$ decrease, $\Delta E^0 (= E_2^0 - E_1^0)$ increases, and/or the rate



Scheme 2. Flowchart of the protocol proposed for the determination of the heterogeneous rate constant and the formal potentials of the two ETs from the key features of the experimental CV signal of an EE_{irr} mechanism for the case $R_k \neq 0$, with $\alpha = 0.5$ and $T = 298.15$ K. (*) Given the number of unknown parameters, an independent determination of ΔE^0 is necessary. Thus, by decreasing the scan rate so that the reversible behavior is approached, the ΔE^0 -value can be determined from $\Delta E_{peak,rev}$ (two peaks) and/or $W_{1/2,rev}$ (two or one peak) (black curves in Figs. 2b and 3b).

constant of the second transfer is higher than the first one (*i.e.*, as R_k increases). Hence, EE processes showing inverted ordering of formal potentials will reach the irreversible behavior ‘easier’ than those with normal ordering.

CRedit authorship contribution statement

Manuela López-Tenés: Conceptualization, Methodology, Software, Writing – original draft. **Joaquín González:** Formal analysis, Software, Writing – original draft, Project administration. **Eduardo Laborda:** Methodology, Software, Writing – original draft. **Angela Molina:** Conceptualization, Methodology, Writing – original draft, Project administration.

Declaration of Competing Interest

The authors declare that they have no known competing financial interests or personal relationships that could have appeared to influence the work reported in this paper.

Data availability

Data will be made available on request.

Acknowledgments

The authors greatly appreciate the financial support provided by the Ministerio de Ciencia e Innovación (PID2019–106097GB-I00/AEI/10.13039/501100011033), as well as by MCIN/AEI/10.13039/501100011033 and the European Union “NextGenerationEU”/PRTR” through the project TED2021–130334B-I00.

Supplementary materials

Supplementary material associated with this article can be found, in the online version, at [doi:10.1016/j.electacta.2023.142694](https://doi.org/10.1016/j.electacta.2023.142694).

References

- [1] P.N. Bartlett, *Bioelectrochemistry: Fundamentals, Experimental Techniques and Applications*, John Wiley & Sons Inc, 2008, <https://doi.org/10.1002/9780470753842>.
- [2] L. Luan, X. Ji, B. Guo, J. Cai, W. Dong, Y. Huang, S. Zhang, Bioelectrocatalysis for CO₂ reduction: recent advances and challenges to develop a sustainable system for CO₂ utilization, *Biotechnol. Adv.* 63 (2023), 108098, <https://doi.org/10.1016/j.biotechadv.2023.108098>.
- [3] L.F.T. Novaes, J. Liu, Y. Shen, L. Lu, J.M. Meinhardt, S. Lin, Electrocatalysis as an enabling technology for organic synthesis, *Chem. Soc. Rev.* 50 (2021) 7941–8002, <https://doi.org/10.1039/d1cs00223f>.
- [4] N. Kaeffer, W. Leitner, Electrocatalysis with molecular transition-metal complexes for reductive organic synthesis, *JACS Au* 2 (2022) 1266–1289, <https://doi.org/10.1021/JACS.2C00031>. <https://doi.org/10.1021/JACS.2C00031>/ASSET/IMAGES/LARGE/AU2C00031_0018.JPEG.
- [5] K.J. Lee, B.D. McCarthy, J.L. Dempsey, On decomposition, degradation, and voltammetric deviation: the electrochemist’s field guide to identifying precatalyst transformation, *Chem. Soc. Rev.* 48 (2019) 2927–2945, <https://doi.org/10.1039/c8cs00851e>.
- [6] E. Martínez-González, C. Amador-Bedolla, V.M. Ugalde-Saldivar, Reversible redox chemistry in a phenoxazine-based organic compound: a two-electron storage negolyte for alkaline flow batteries, *ACS Appl. Energy Mater.* 5 (2022) 14748–14759, <https://doi.org/10.1021/ACS.AEM.2C02114>. <https://doi.org/10.1021/ACS.AEM.2C02114>/SUPPL_FILE/AE2C02114_SI_001.PDF.
- [7] M.C. McCormick, K. Keijzer, A. Polavarapu, F.A. Schultz, M.H. Baik, Understanding intrinsically irreversible, non-nernstian, two-electron redox processes: a combined experimental and computational study of the electrochemical activation of Platinum(IV) antitumor prodrugs, *J. Am. Chem. Soc.* 136 (2014) 8992–9000, <https://doi.org/10.1021/ja5029765>.
- [8] M. Mohammad, A. Rauf, S. Rauf, An electrochemical and computational analysis of electronic communication in a “molecular spider”, *ChemistrySelect* 2 (2017) 3690–3694, <https://doi.org/10.1002/slct.201700317>.
- [9] K.J. Lee, N. Elgrishi, B. Kandemir, J.L. Dempsey, Electrochemical and spectroscopic methods for evaluating molecular electrocatalysts, *Nat. Rev. Chem.* 1 (2017) 0039, <https://doi.org/10.1038/s41570-017-0039>.
- [10] S. Fukuzumi, Y.M. Lee, W. Nam, Immobilization of molecular catalysts for enhanced redox catalysis, *ChemCatChem* 10 (2018) 1686–1702, <https://doi.org/10.1002/cctc.201701786>.
- [11] R.M. Bullock, A.K. Das, A.M. Appel, Surface immobilization of molecular electrocatalysts for energy conversion, *Chem. A Eur. J.* 23 (2017) 7626–7641, <https://doi.org/10.1002/chem.201605066>.
- [12] A.J. Bard, L.R. Faulkner, H.S. White, *Electrochemical Methods: Fundamentals and Applications*, 3rd Edition, John Wiley & Sons, Ltd, 2022.
- [13] A. Molina, J. González, *Pulse Voltammetry in Physical Electrochemistry and Electroanalysis*, Springer International Publishing, Berlin, 2016, <https://doi.org/10.1007/978-3-319-21251-7>.
- [14] E. Laviron, Voltammetric methods for the study of adsorbed species, in: A.J. Bard (Ed.), *Electroanal. Chem. Vol. 12*, Marcel Dekker, New York, 1982, pp. 53–157.
- [15] R.F. Lane, A.T. Hubbard, Electrochemistry of chemisorbed molecules. I. Reactants connected to electrodes through olefinic substituents, *J. Phys. Chem.* 77 (1973) 1401–1410, <https://doi.org/10.1021/j100630a018>.
- [16] E. Laviron, General expression of the linear potential sweep voltammogram in the case of diffusionless electrochemical systems, *J. Electroanal. Chem.* 101 (1979) 19–28, [https://doi.org/10.1016/S0022-0728\(79\)80075-3](https://doi.org/10.1016/S0022-0728(79)80075-3).
- [17] J.C. Myland, K.B. Oldham, Quasireversible cyclic voltammetry of a surface confined redox system: a mathematical treatment, *Electrochem. Commun.* 7 (2005) 282–287, <https://doi.org/10.1016/j.elecom.2005.01.005>.
- [18] J. Waelder, S. Maldonado, Beyond the laviron method: a new mathematical treatment for analyzing the faradaic current in reversible, quasi-reversible, and irreversible cyclic voltammetry of adsorbed redox species, *Anal. Chem.* 93 (2021) 12672–12681, <https://doi.org/10.1021/acs.analchem.1c02503>.
- [19] M. Robinson, K. Ounnunkad, J. Zhang, D. Gavaghan, A. Bond, Integration of heuristic and automated parametrization of three unresolved two-electron surface-confined polyoxometalate reduction processes by AC voltammetry, *Chemelectrochem* 5 (2018) 3771–3785, <https://doi.org/10.1002/celec.201800950>.
- [20] A.R. Dale-Evans, M.J. Robinson, H.O. Lloyd-Laney, D.J. Gavaghan, A.M. Bond, A. Parkin, A voltammetric perspective of multi-electron and proton transfer in protein redox chemistry: insights from computational analysis of *Escherichia coli* HypD fourier transformed alternating current voltammetry, *Front. Chem.* 9 (2021), 672831, <https://doi.org/10.3389/fchem.2021.672831>.
- [21] V. Mirceski, R. Gulaboski, A theoretical and experimental study of a two-step quasireversible surface redox reaction by square-wave voltammetry, *Croat. Chem. Acta.* 76 (2003) 37–48.
- [22] R. Gulaboski, P. Kokoškarova, S. Mitrev, Theoretical aspects of several successive two-step redox mechanisms in protein-film cyclic staircase voltammetry, *Electrochim. Acta.* 69 (2012) 86–96, <https://doi.org/10.1016/j.electacta.2012.02.086>.
- [23] J. Gonzalez, M. López-Tenés, A. Molina, Non-nernstian two-electron transfer reactions for immobilized molecules: a theoretical study in cyclic voltammetry, *J. Phys. Chem. C* 117 (2013) 5208–5220, <https://doi.org/10.1021/jp312621u>.
- [24] D.H. Evans, K. Hu, Inverted potentials in two-electron processes in organic electrochemistry, *J. Chem. Soc. Faraday Trans.* 92 (1996) 3983–3990, <https://doi.org/10.1039/r9969203983>.
- [25] K. Tammeveski, K. Kontturi, R.J. Nichols, R.J. Potter, D.J. Schiffrin, Surface redox catalysis for O₂ reduction on quinone-modified glassy carbon electrodes, *J. Electroanal. Chem.* 515 (2001) 101–112, [https://doi.org/10.1016/S0022-0728\(01\)00633-7](https://doi.org/10.1016/S0022-0728(01)00633-7).
- [26] F. Baymann, B. Schoepp-Cothenet, S. Duval, M. Guiral, M. Brugna, C. Baffert, M. J. Russell, W. Nitschke, On the natural history of flavin-based electron bifurcation, *Front. Microbiol.* 9 (2018) 1357, <https://doi.org/10.3389/fmicb.2018.01357>.
- [27] J. Gonzalez, J.A. Coca-Clemente, A. Molina, E. Laborda, J.M. Gomez-Gil, L. A. Rincon, Carbon support effects and mechanistic details of the electrocatalytic activity of polyoxometalates investigated via square wave voltacoulometry, *ACS Catal.* 7 (2017) 1501–1511, <https://doi.org/10.1021/acscatal.6b03392>.
- [28] A.R. Dale-Evans, M.J. Robinson, H.O. Lloyd-Laney, D.J. Gavaghan, A.M. Bond, A. Parkin, A voltammetric perspective of multi-electron and proton transfer in protein redox chemistry: insights from computational analysis of *Escherichia coli* hypd fourier transformed alternating current voltammetry, *Front. Chem.* 9 (2021) 424, <https://doi.org/10.3389/fchem.2021.672831>.
- [29] M.C. Henstridge, E. Laborda, N.V. Rees, R.G. Compton, Marcus-Hush-Chidsey theory of electron transfer applied to voltammetry: a review, *Electrochim. Acta.* 84 (2012) 12–20, <https://doi.org/10.1016/j.electacta.2011.10.026>.
- [30] M. López-Tenés, J. Gonzalez, A. Molina, Two-electron transfer reactions in electrochemistry for solution-soluble and surface-confined molecules: a common approach, *J. Phys. Chem. C* 118 (2014) 12312–12324, <https://doi.org/10.1021/jp5025763>.